



# 1 **Response of the link between ENSO and the East Asian winter** 2 **monsoon to Asian anthropogenic aerosols**

3 Zixuan Jia<sup>1</sup>, Massimo A Bollasina<sup>2</sup>, Wenjun Zhang<sup>1</sup>, Ying Xiang<sup>3</sup>

4

5 <sup>1</sup>School of Atmospheric Science, Nanjing University of Information Science and Technology, Nanjing, China

6 <sup>2</sup>School of GeoSciences, University of Edinburgh, Edinburgh, UK

7 <sup>3</sup>Jiangsu Climate Center, Nanjing, China

8

9 *Correspondence to:* Zixuan Jia (zx.jia@nuist.edu.cn)

10 **Abstract.** We use coupled and atmosphere-only simulations from the Precipitation Driver and  
11 Response Model Intercomparison Project to investigate the impacts of Asian anthropogenic sulfate  
12 aerosols on the link between the El Niño-Southern Oscillation (ENSO) and the East Asian Winter  
13 monsoon (EAWM). In fully-coupled simulations, aerosol-induced cooling extends southeastward to the  
14 Maritime Continent and the north-western Pacific. Remotely, this broad cooling weakens the easterly  
15 trade winds over the central Pacific, which reduces the east-west equatorial Pacific sea surface  
16 temperature gradient. These changes contribute to increasing ENSO's amplitude by 17%, mainly  
17 through strengthening the zonal wind forcing. Concurrently, the El Niño-related warm SST anomalies  
18 and the ensuing Pacific-East Asia teleconnection pattern (i.e. the ENSO-EAWM link) intensify, leading  
19 to an increased EAWM amplitude by 18% in the coupled simulations. Therefore, in response to the  
20 increasing frequency of El Niño and La Niña years under Asian aerosol forcing, the interannual  
21 variability of the EAWM increases, with more extreme EAWM years. The opposite variations in the  
22 interannual variability of the EAWM to Asian aerosols in atmosphere-only simulations (-19%) further  
23 reflect the importance of ENSO-related atmosphere-ocean coupled processes. A better understanding  
24 of the changes of the year-to-year variability of the EAWM in response to aerosol forcing is critical to  
25 reducing uncertainties in future projections of variability of regional extremes, such as cold surges and  
26 flooding, which can cause large social and economic impacts on densely populated East Asia.

## 27 **1 Introduction**

28 The East Asian winter monsoon (EAWM) is one of the most prominent features of the northern  
29 hemisphere atmospheric circulation during the boreal winter, and has a pronounced influence on  
30 weather and climate of the Asian-Pacific region from the northern latitudes to the equator (e.g. Chang,  
31 2006). As such, variations of the EAWM have the potential to cause extreme cold disasters and severe  
32 flooding in Southeast Asian countries (e.g. Feng et al. 2010; Huang et al. 2012), with consequent marked  
33 social and economic impacts (e.g. Chen et al., 2005; Zhou et al. 2011). Thus, it is very important to



1 understand the mechanisms underpinning its variability and associated drivers, and to ultimately  
2 develop more robust projections of its future evolution.

3

4 The EAWM is fundamentally driven by the thermal contrast between the cold Asian continent and the  
5 adjacent warm oceans (e.g. Yang et al., 2002; Huang et al., 2012; Chen et al., 2019). Its climatological  
6 pattern is mainly characterized by dry cold low-level northwesterlies along the eastern flank of the  
7 Siberian High and low-level northeasterlies along the coast of East Asia, triggering cold air outbreaks  
8 in northern China and generating cold surges over southern China as well as the South China Sea (Li  
9 and Wang, 2012; He et al., 2013). The EAWM exhibits distinct interannual variability (e.g. Gong et al.,  
10 2014), which is strongly influenced by the El Niño-Southern Oscillation (ENSO) and the ensuing  
11 Pacific-East Asia (PEA) teleconnection pattern (e.g. Zhang et al., 1996). Associated with an El Niño  
12 event, the anomalous anticyclone over the western tropical Pacific (the most remarkable low-level  
13 circulation feature of the PEA) induces southwesterlies on its western flank, which weaken the EAWM  
14 flow and lead to warmer and wetter conditions over southeastern China and the South China Sea (Wang  
15 et al., 2000, 2013). In turn, the EAWM tends to be strong during La Niña winters, with widespread  
16 cooling and reduced precipitation.

17

18 Previous studies indicated that magnitude and location of ENSO-induced teleconnection patterns are  
19 influenced by ENSO characteristics, such as amplitude and location of its sea surface temperature (SST)  
20 anomalies (Cai et al., 2021; Jiang et al., 2022). However, future projections of ENSO characteristics are  
21 highly uncertain, even in the latest CMIP6 models (Huang and Xie, 2015; Yan et al., 2020; Beobide-  
22 Arsuaga et al., 2021). Therefore, there is no consensus on future changes in the ENSO-induced  
23 teleconnections, including projections of the PEA pattern (e.g. Wang et al., 2013; Jia et al., 2020). The  
24 characteristics of ENSO and its induced atmospheric teleconnections are closely related to the tropical  
25 Pacific mean state via ocean-atmosphere feedbacks (Jin, 1997; Wang, 2002; Cai et al., 2014). Based on  
26 ocean-atmosphere reanalyses, observed mean state changes since the 1980s feature a La Niña-like  
27 warming (i.e. the tropical Pacific warming center is mainly located in the western basin; Rayner et al.,  
28 2003; Kobayashi et al., 2015; Huang et al., 2017). However, both a La Niña-like and an El Niño-like  
29 warming (i.e. tropical Pacific warming centered in the eastern basin) are projected in the future, with a  
30 large spread across different climate models (e.g. Power et al., 2013; Lian et al., 2018). These two  
31 different warming patterns will cause a corresponding strengthening and weakening of the easterly trade  
32 winds over the tropical Pacific Ocean, respectively, resulting in opposite changes in the characteristics  
33 of ENSO (Vecchi et al., 2006; Collins et al., 2010). While the majority of the studies have focused on  
34 the influence of increasing greenhouse gas concentrations on the tropical Pacific mean state (e.g. Wang  
35 et al., 2017; Yan et al., 2020), the impact of anthropogenic aerosols has been largely overlooked.

36



1 Due to the intensification of human industrial activities, the global mean atmospheric burden of  
2 anthropogenic aerosols has continued to increase over the past century, exerting a significant imprint  
3 on worldwide climate (Liao et al., 2015; Forster et al., 2021; Persad, 2023). Anthropogenic aerosols can  
4 affect climate by modulating shortwave radiation and, to some extent, longwave radiation directly, and  
5 through their interactions with clouds and precipitation indirectly (Boucher et al., 2013; Myhre et al.,  
6 2013; Zhao and Suzuki, 2019). Unlike greenhouse gases, which are distributed evenly across the globe,  
7 anthropogenic aerosols reside in the atmosphere for a short time (days to weeks) due to numerous  
8 chemical and physical removal processes, which causes their distribution and associated radiative  
9 forcing to be spatially heterogeneous (Allen et al., 2015; Wilcox et al., 2019). As such, aerosols can  
10 induce substantial changes in local atmospheric circulation and extend their influence over long  
11 distances, even over the surrounding ocean, triggering ocean–atmosphere interactions (Rotstayn and  
12 Lohmann, 2002; Ramanathan et al., 2005; Westervelt et al., 2020). Some studies indicated that the  
13 influence of anthropogenic aerosols from remote sources can even outweigh that of locally-emitted ones  
14 (Shindell et al., 2012; Lewinschal et al., 2013). Since the start of the industrial age, vast emissions of  
15 aerosols and their precursors over the Northern Hemisphere have had a profound cooling effect, and  
16 this preferential cooling has been linked to a southward shift of the Intertropical Convergence Zone (e.g.  
17 Hwang et al., 2013; Navarro et al., 2017).

18

19 The emissions of anthropogenic aerosols and their precursors in Asia have increased rapidly since 1980,  
20 and many studies have focused on Asian as well as Northern Hemispheric climate (e.g. Bollasina et al.,  
21 2014; Bartlett et al., 2018; Wilcox et al., 2019; Li et al., 2022). While Asian anthropogenic aerosols can  
22 significantly affect the Asian monsoon, the large majority of the current literature has focused on the  
23 effects of aerosols on the summer or annual mean climatology (e.g., Westervelt et al., 2018; Song et al.,  
24 2014; Persad et al., 2022). Only a limited number of studies have focused on the influence of aerosols  
25 on the EAWM (Jiang et al., 2017; Liu et al., 2019; Wilcox et al., 2019), while their effect on the  
26 interannual variability of the EAWM and the link to ENSO remains unexplored. In boreal winter, coal  
27 and fossil fuels are combusted intensively across Asia (Gao et al., 2018; Cheng et al., 2019), setting the  
28 stage for a potential important influence on continental climate and the mean EAWM circulation.  
29 Moreover, ENSO and the associated PEA teleconnection pattern peak in the winter, representing a  
30 major driver of interannual fluctuations of the EAWM. The extent to which aerosols may affect ENSO  
31 and the related ocean-atmosphere feedbacks has not been thoroughly investigated and is unclear  
32 (Westervelt et al., 2018; Wilcox et al., 2019). Given the rapid variations in aerosol emissions over Asia,  
33 addressing this knowledge gap is both compelling and timely for enhancing our understanding and  
34 projections of the ENSO-EAWM link in the near future, and potential causes of changes in the  
35 interannual variability of the EAWM.

36



1 In this study, we use multi-model mean data from regional aerosol perturbation experiments conducted  
2 with coupled and atmosphere-only models (Section 2) to investigate the impacts of Asian aerosols on  
3 the ENSO-EAWM link and the interannual variability of the EAWM (Section 3). We then link changes  
4 in the PEA pattern to the remote impacts of Asian aerosols on ENSO (Section 4). Mechanisms driving  
5 changes in the tropical Pacific mean state and ENSO characteristics are further investigated in Section  
6 5. Finally, Section 6 summarises the main results and provides key conclusions.

## 7 **2 Data and methodology**

8 Model data from the Precipitation Driver and Response Model Intercomparison Project (PDRMIP;  
9 Myhre et al., 2017) are used to investigate the impact of Asian anthropogenic aerosols on the ENSO-  
10 EAWM link. PDRMIP offers a unique opportunity for elucidating the complexities of the slow and fast  
11 responses of the EAWM to Asian aerosols and the contribution of ENSO-related ocean-atmosphere  
12 coupled processes with coupled and atmosphere-only simulations by comparing baseline and regional  
13 aerosol perturbation experiments. The baseline simulation was forced by present-day (year 2000) levels  
14 of aerosols and greenhouse gas emissions/concentrations. The regional aerosol experiment analysed in  
15 this study has sulfate concentrations/emissions over Asia (10°–50°N, 60°–140°E) increased by a factor  
16 of 10 compared to the baseline values (hereafter SUL×10Asia). Note that sulfate is the predominant  
17 aerosol component in boreal winter over Asia (e.g. Liu et al., 2009; Zhang et al., 2018). The response  
18 to Asian aerosols is identified as the difference between the SUL×10Asia and the baseline experiments.  
19 Of the 10 models that contributed to PDRMIP, seven performed the SUL×10Asia experiment: GISS-  
20 E2, HadGEM3-GA4, IPSL-CM5A, MIROC-SPRINTARS, ESM1-CAM4, CESM1-CAM5, and  
21 NorESM1 (details on the resolution and aerosol setup for each model can be found in Table 1 of Liu et  
22 al. (2018)). For each model and experiment, a pair of simulations was performed: one in a fully coupled  
23 atmosphere–ocean setting (called “coupled”), and one with fixed climatological sea surface  
24 temperatures (called fSST). The coupled simulations were run for 100 years and the fSST simulations  
25 for 15 years. The concentrations of all non-aerosol anthropogenic forcings and natural forcing were kept  
26 at present-day levels (typically year 2000) in all the experiments, as are the SSTs for the fSST  
27 simulations. In this study, we use output from the last 50 winters (DJF, December of the current year  
28 and January and February of the following year) of coupled simulations and the last 12 winters of the  
29 fSST simulations to discard the model spin-up time and consistently with existing literature (Liu et al.,  
30 2018; Dow et al., 2021; Fahrenbach et al., 2024).

31

32 Reanalysis and observational data for DJF 1965–2014 (50 years) are used to evaluate the PDRMIP-  
33 simulated EAWM and ENSO-related patterns in the baseline experiment. Monthly meteorological  
34 reanalysis data are from the fifth-generation atmospheric reanalysis ERA5 provided by the European  
35 Centre for Medium-Range Weather Forecasts at a spatial resolution of 0.25° (Copernicus Climate



1 Change Service, 2017; Hersbach et al., 2023). Monthly gridded observations are from the Hadley Centre  
2 Sea Ice and Sea Surface Temperature (HadISST) dataset for sea surface temperature at a spatial  
3 resolution of  $1^\circ$  (Rayner et al., 2003), and from the Climatic Research Unit (CRU) v4.07 data set for  
4 land surface temperature with a spatial resolution of  $0.5^\circ$  (Harris et al., 2020). To quantify the EAWM  
5 interannual variability, we use the Ji et al. (1997) index (the negative 1000 hPa meridional wind  
6 anomaly averaged over  $10^\circ\text{--}30^\circ\text{N}$ ,  $115^\circ\text{--}130^\circ\text{E}$ ) as it represents the spatio-temporal characteristics of  
7 the ENSO–EAWM relationship well (Gong et al., 2015; Jia et al., 2020). Positive values indicate a  
8 stronger-than-normal EAWM. ENSO is described by the Niño3.4 index (area-averaged SST anomaly  
9 over  $5^\circ\text{S}\text{--}5^\circ\text{N}$ ,  $120^\circ\text{--}170^\circ\text{W}$ ). The ENSO-related PEA pattern is deduced by regression analysis, and  
10 the statistical significance is evaluated using the two-tailed Student’s *t*-test. Among the seven PDRMIP  
11 models with the SUL $\times$ 10Asia experiment, coupled baseline simulations in CESM1-CAM5, MIROC-  
12 SPRINTARS, HadGEM3-GA4, and NorESM1 can well capture the observed pattern and magnitude of  
13 the ENSO-related circulation anomalies across East Asia and the Pacific (Fig. S1) and are used in this  
14 study. These four models include parameterisations of both aerosol-radiation and aerosol-cloud  
15 interactions, while the others don’t include indirect effects, or include only the first indirect effect (Liu  
16 et al., 2018; Dow et al., 2021). (Table 1). All the data are interpolated to a  $3.75^\circ \times 2^\circ$  (longitude  $\times$   
17 latitude) resolution before the analysis for consistency between all models.

18

### 19 **3 Impacts of Asian aerosols on the PEA pattern and the EAWM interannual variability**

20 The ENSO-related circulation and precipitation anomalies across East Asia and the Pacific (i.e. the PEA  
21 pattern) (Figs. 1a-c) are well reproduced by the multi-model mean of the PDRMIP coupled baseline  
22 simulations (Figs. 1d-f). The pattern is characterised by the El Niño-related warm SST anomalies over  
23 the equatorial Pacific and cold SSTs over the north-western Pacific (Fig. 1a), the anomalous anticyclone  
24 over the western tropical Pacific and the anomalous low over the northern extratropical Pacific (Fig.  
25 1b). On the western flank of the anticyclone, near-surface and lower tropospheric southerly winds along  
26 the East Asian coast (Figs. 1a-b) lead to warm surface air temperature and precipitation over  
27 southeastern China and even over central China (Figs. 1a, c), while the lower tropospheric northerly  
28 winds on the western flank of the cyclone bring cold air to northeastern China (Fig. 1b). The spatial  
29 patterns of simulated anomalies are broadly similar to those found in observations, including the  
30 position and magnitude of El Niño-related warm SST anomalies, anticyclone and cyclone anomalies,  
31 and precipitation anomalies (Figs. 1d-f). The multi-model mean from PDRMIP shares common biases  
32 with other CMIP5 and CMIP6 models, such as a slightly westward shift of the equatorial Niño warming  
33 with associated circulation and precipitation anomalies (Gong et al., 2015; Wang et al., 2022). Overall,  
34 the multi-model mean coupled PDRMIP baseline simulations successfully reproduce the PEA pattern.

35



1 In response to Asian aerosols, the El Niño-related warm SST anomalies intensify over the eastern  
2 equatorial Pacific, associated with an intensification of the anomalous SST cooling over the western  
3 tropical Pacific (Figs. 1d, g). Concurrently, the anticyclonic anomalies over the western tropical Pacific  
4 strengthen and stretch northwestward, while the cyclone over the northern Pacific strengthens and  
5 covers a broader region (Figs. 1e, h). This enhanced anticyclone results in an intensification of southerly  
6 anomalies along the Asian coast from the South China Sea (Figs. 1g-h), advecting warm and humid air  
7 (Figs. 1f, i). Over land, warm and wet anomalies over southeastern and central China weaken, as well  
8 as cold anomalies over northeastern China (Figs. 1d, f, g, i), consistent with the changes in the  
9 atmospheric circulation patterns mentioned above. Overall, these changes suggest that the ENSO signal  
10 and its induced PEA pattern enhance under increased Asian aerosols. Given the interannual variability  
11 of the EAWM is strongly influenced by the PEA pattern, the intensification of southerly anomalies  
12 along the Asian coast associated with the enhanced PEA may lead to an increase in the interannual  
13 variability of the EAWM.

14

15 Changes in the interannual variability of the EAWM in response to Asian aerosol increase are shown  
16 by the probability distributions of the EAWM index (Fig. 2). The simulated amplitude of the EAWM  
17 (defined as the standard deviation of the EAWM index) is smaller than the observed amplitude in  
18 baseline simulations, which is a general known bias in models (Wang et al., 2010; Gong et al., 2014).  
19 In coupled simulations, the multi-model mean EAWM amplitudes are 0.55 and 0.65  $\text{m s}^{-1}$  for the  
20 baseline and SUL×10Asia experiments, respectively, indicating an 18% increase due to the Asian  
21 aerosols, together with more extreme EAWM years in the SUL×10Asia experiment (Fig. 2a). These  
22 changes are consistent with the aerosol-enhanced PEA pattern identified above. However, in fSST  
23 simulations, the multi-model mean EAWM amplitude decreases by 19%, accompanied by more strong-  
24 EAWM years and less weak-EAWM years in SUL×10Asia experiments (Fig. 2b). These changes can  
25 be explained by aerosol-induced cooling over the emission region and the formation of an anomalous  
26 anticyclonic circulation (e.g. Hu et al., 2015; Liu et al., 2019; Dow et al., 2021), and indicate an  
27 enhanced climatological pattern of the EAWM under increased aerosols (Figs. S2a-f). In addition to  
28 this atmospheric-only response, the influence of Asian aerosols can extend over the Maritime Continent  
29 and the north-western Pacific (Wilcox et al., 2019; Dow et al., 2021). In coupled simulations, the  
30 climatological pattern of the EAWM extends southeasterly, which is mainly represented by an  
31 anomalous anticyclone centred over the southwest of the Philippines (Figs. S2g-i). This anomalous  
32 anticyclone, attributed to the southward shift of the Hadley circulation to compensate for the  
33 interhemispheric asymmetry in aerosol radiative cooling (Liu et al., 2019), enhances the northerlies  
34 over the Maritime Continent but slightly weakens the northerlies along the East Asian coast (Figs. S2g-  
35 h). This pattern cannot explain the increased interannual variability of the EAWM in coupled  
36 simulations as it is not associated with an evident modulation of the climatological monsoon flow. The  
37 EAWM-related circulation and precipitation anomalies brought about by increased aerosols in the



1 coupled experiments (Fig. S3) feature an enhanced PEA pattern. This further suggests the contribution  
2 of the enhanced ENSO-induced PEA pattern to increased interannual variability of the EAWM. The  
3 opposite variations in the interannual variability of the EAWM to Asian aerosols in fully coupled  
4 experiments and atmosphere-only (+18% and -19%, respectively) also reflect the importance of ENSO-  
5 related atmosphere-ocean coupled processes.

#### 6 **4 The response of ENSO amplitude to increased Asian aerosols**

7 Following previous studies (e.g. Wang et al., 2013; Wang et al., 2022), the increased ENSO signal and  
8 its induced teleconnection pattern can be further linked to changes in the ENSO amplitude (defined as  
9 the standard deviation of the Niño3.4 index). Figure 3a shows the observed standard deviation of SST  
10 across the tropical Pacific, with the highest values over the central-eastern equatorial Pacific. This  
11 spatial pattern is well captured by the multi-model mean in the coupled baseline simulation (Fig. 3b),  
12 albeit the core values are slightly underestimated in magnitude and spatial extent, especially in the  
13 meridional direction. Increased aerosols lead to significant increases in the SST standard deviation over  
14 the Maritime Continent and the central-eastern equatorial Pacific (Fig. 3c). This is consistent with the  
15 increased ENSO signal and the related changes in SST anomalies over these two regions (Fig. 1g).  
16 Figure 3d shows the probability distributions of the Niño3.4 index from the coupled baseline (blue curve  
17 and shading) and SUL×10Asia (red curve and shading) simulations. The multi-model mean ENSO  
18 amplitude increases by 17% under aerosol forcing (from 0.7 °C to 0.82 °C).

19

20 Consistently with the increased ENSO amplitude, Table 1 shows that there are more El Niño (Niño3.4  
21 index > 0.5 °C) and La Niña (the Niño3.4 index < -0.5 °C) years in the coupled SUL×10Asia simulation  
22 compared to the baseline for each model, with the increase up to 100% (from 14 to 28 events in the 50-  
23 year record). Figure 4 shows the joint distributions of multi-model mean aerosol-driven changes in the  
24 Niño3.4 index compared with the EAWM index in coupled simulations. Both the Niño3.4 index and  
25 the EAWM index have a wide range of variations (i.e. from -1.5 to 1.5 °C and -1 to +1 m s<sup>-1</sup> respectively),  
26 suggesting that both the ENSO amplitude and the interannual variability of the EAWM increase under  
27 Asian aerosol forcing as indicated above. Remarkably, changes in the Niño3.4 index are significantly  
28 anti-correlated ( $p < 0.01$ ) with those in the EAWM index ( $r = -0.38$ ). In particular, when the Niño3.4  
29 index decreases by less than 0.5 °C due to Asian aerosol forcing, the EAWM is 2.5 times more likely to  
30 strengthen than weaken, and vice versa. This is consistent with the negative relationship between ENSO  
31 and the EAWM induced by the ensuing PEA teleconnection pattern (Wang et al., 2000). These results  
32 show that Asian aerosols lead to an increase in the ENSO amplitude, resulting in increased interannual  
33 variability of the EAWM through the associated PEA pattern.





## 1 **5 Changes in the tropical Pacific mean state and ocean-atmosphere feedbacks**

2 It is well-known that ENSO is fundamentally governed by ocean-atmosphere coupled processes in the  
3 tropical Pacific (Timmermann et al., 2018; Rashid et al., 2022). It is therefore interesting to examine  
4 how the tropical Pacific mean state and atmosphere-ocean coupling are affected by Asian aerosol  
5 forcing. Figure 5 shows the climatological annual variation of key surface variables across the  
6 equatorial Pacific Ocean in the coupled baseline simulation and their changes under increased Asian  
7 aerosols. In the baseline simulation, the equatorial Pacific mean state is characterised by easterly trade  
8 winds with maximum magnitude over the central-eastern Pacific, an east-west SST gradient, and strong  
9 SST amplitudes (i.e. standard deviations of SST) over the eastern Pacific (Figs. 5a-c). These features  
10 are altered in the SUL×10Asia experiment relative to the baseline experiment, with significant seasonal  
11 differences. In particular, anomalous westerlies develop from spring over the eastern Pacific, then  
12 gradually strengthen until the peak in September while moving towards the central Pacific (the Niño4  
13 region, purple bar) (Fig. 5d). Westerly wind anomalies are considered to play an important role during  
14 the development stage (i.e. boreal autumn) of ENSO events, by generating warm SST anomalies in the  
15 eastern equatorial Pacific via the thermocline and the advective feedbacks (McPhaden, 1999; Lian and  
16 Chen, 2021; Xuan et al., 2024). This anomalous westerly flow weakens the climatological easterly trade  
17 winds in the coupled SUL×10Asia simulation compared to the baseline (Figs. 5a, d). Furthermore,  
18 anomalous SST warming appears over the eastern Pacific (the Niño3 region, green bar) from autumn  
19 to winter (peak around October) (Fig. 5e), which decreases the east-west equatorial Pacific SST gradient  
20 (Fig. 5b). Note that Figures 5b and 5e show SST minus zonal mean and SST difference minus zonal  
21 mean respectively to clarify the east-west SST changes gradient. Given the broad aerosol-induced  
22 cooling over the Pacific (Fig. S2h), warming SST anomalies on Figure 5e represent less cooling.  
23 Correspondingly, the SST amplitude increases with maximum values in the winter mainly over the  
24 central-eastern Pacific (the Niño3.4 region) (Fig. 5f), which is consistent with the increased ENSO  
25 amplitude under Asian aerosol forcing indicated above. Previous studies have found a link between  
26 warmer SST in the eastern than in the western equatorial Pacific with an increase in ENSO amplitude  
27 (Zheng et al., 2016; Ying et al., 2019; Hayashi et al., 2020).

28

29 Given the above marked changes over the equatorial Pacific mean state occur in autumn and winter, we  
30 further explore the response of the tropical Pacific mean state to Asian aerosols in these two seasons.  
31 In autumn (SON, September-October-November), there are a zonally wider anticyclone, cooling and  
32 negative precipitation anomalies stretching from Asia to the whole North Pacific (Figs. 6a-c) compared  
33 to those in winter (Figs. 6d-f). As in Figure 5e, Figure 6b and 6c show surface air temperature (SST  
34 over the ocean) difference minus domain mean, on which warming SST anomalies represent less  
35 cooling. These differences between SON and DJF are related to the climatological pattern in SON when  
36 the Siberian High is close to the broad North Pacific subtropical high and the Aleutian Low is weak





1 (Fig. S4), that lead to the zonally wider cooling by Asian aerosols. The cooling and associated  
2 anticyclonic anomalies trigger cross-equatorial wind anomalies from the Northern Hemisphere to the  
3 Southern Hemisphere, which shift the ITCZ southward (Figs. 6a-c), as indicated by previous studies on  
4 the interhemispheric difference in aerosol emissions (Navarro et al., 2017; Voigt et al., 2017; Wilcox et  
5 al., 2019). Deflected by the Coriolis force, the cross-equatorial wind anomalies present a westerly  
6 anomaly near the equator mainly over the central Pacific (purple box in Fig. 6a), which can weaken the  
7 easterly trade winds, generating warm SST anomalies over the eastern Pacific (green box in Fig. 6b)  
8 and excess rainfall (Fig. 6c). From SON to DJF, the climatological Siberian High strengthens, and the  
9 Aleutian Low deepens with a southward shift in the coupled baseline simulation (Figs. S4a, S2a).  
10 Therefore, the Asian aerosol-induced cooling and associated anticyclone are more concentrated over  
11 the Maritime Continent and the north-western Pacific (Fig. 6d), altering the SST gradient anomaly from  
12 north-south (Fig. 6b) to northwest-southeast (Fig. 6e). This SST anomaly pattern leads to the southward  
13 shift of anomalous westerly winds over the central-eastern Pacific, as well as warm SST and positive  
14 precipitation anomalies over eastern Pacific (Figs. 6d-f). These anomalies are conducive to increasing  
15 the ENSO amplitude.

16

17 The processes that most significantly contribute to ENSO are surface wind responses to the equatorial  
18 eastern Pacific SST variations (the Bjerknes or zonal wind feedback), the zonal advection of mean SSTs  
19 by the anomalous current (the zonal advective feedback) and the vertical advection of anomalous  
20 subsurface temperatures by the mean upwelling (the thermocline feedback). The two latter feedbacks  
21 are related to the ocean dynamic responses to zonal wind forcing that cause in-phase variations of  
22 eastern Pacific SST anomalies (Jin and An, 1999; Kim et al., 2014). A diagnostic quantity that includes  
23 both these two feedback processes is the zonal wind forcing of SST anomalies, which was found to be  
24 useful for studying ENSO-amplitude changes under global warming (Rashid et al., 2016). To further  
25 quantify the changes in the strength of the ocean-atmosphere coupling that modulate the ENSO  
26 amplitude, we focus on two main processes, the Bjerknes feedback and zonal wind forcing, which are  
27 related to the formation of the westerly anomalies over the central Pacific and warm SST anomalies  
28 over the eastern Pacific indicated above. Figure 7 shows the lag-regression coefficients between the  
29 SST anomalies averaged over the Niño3 region (green box in Fig. 6b) (the Niño3 SST index) and near-  
30 surface zonal winds (U1000) anomalies averaged over the Niño4 region (purple box in Fig. 6a) (the  
31 Niño4 U1000 index) to represent the Bjerknes feedback and zonal wind forcing. In each panel,  
32 regression coefficients between two variables at different lags are plotted for observations (black curve)  
33 and the coupled baseline (blue curve and shading) and SUL×10Asia (red curve and shading)  
34 simulations. The left panel shows the Niño4 U1000 anomalies response to the Niño3 SST index (i.e.  
35 the Bjerknes feedback). As in most CMIP models (e.g. Bellenger et al., 2014, Rashid et al., 2016), the  
36 simulated Bjerknes feedback is weaker than in observations (Fig. 7a). The strength of the feedback for  
37 lags between -5 and 5 months almost doesn't change in the coupled SUL×10Asia simulation relative



1 to the baseline (Fig. 7a). The right panel shows the Niño3 SST anomalies response to the Niño4 U1000  
2 index (i.e. the zonal wind forcing). In this case, the simulated SST responses are somewhat stronger  
3 than the observed responses, and the maximum responses are found at small positive lags (e.g. when  
4 U1000 leads SST by 1–2 months) (Rashid et al., 2022). The zonal wind forcing, defined as the  
5 maximum of the regression coefficients (lag=1), strengthens from the baseline ( $0.51^{\circ}\text{C m}^{-1}\text{ s}$ ) to the  
6 SUL×10Asia experiment ( $0.55^{\circ}\text{C m}^{-1}\text{ s}$ ) by 8%. Therefore, the zonal wind forcing plays a more  
7 important role than the Bjerknes feedback in increasing the ENSO amplitude under Asian aerosol  
8 forcing. In summary, the Asian aerosol-induced cooling weakens the easterly trade winds over the  
9 central Pacific, which reduces the east-west equatorial Pacific SST gradient through the zonal wind  
10 forcing, leading to increased ENSO amplitude.

## 11 **6 Summary and conclusions**

12 This study investigates the response of the ENSO-EAWM link and related interannual variability of the  
13 EAWM to Asian aerosols, including the induced changes in the ENSO-related ocean-atmosphere  
14 feedbacks, using a set of experiments carried out as part of the PDRMIP initiative. Accounting for two-  
15 way atmosphere-ocean coupling, the El Niño-related warm SST anomalies intensify over the eastern  
16 equatorial Pacific, associated with an enhancement of the anomalous anticyclone anomaly over the  
17 western tropical Pacific and corresponding stronger southerlies along the Asian coast from the South  
18 China Sea. This enhanced ENSO signal and its induced PEA pattern contribute to explaining the  
19 increased interannual variability of the EAWM (+18%). When the ocean is not allowed to respond, the  
20 interannual variability of the EAWM varies in the opposite direction (-19%), which further reflects the  
21 importance of ENSO-related atmosphere-ocean coupled processes for explaining the increased  
22 variability. The PEA-like EAWM-related circulation and precipitation anomalies also hint at a link  
23 between increased interannual variability of the EAWM and changes in ENSO in response to Asian  
24 aerosols. The increased ENSO signal can be further linked to changes in the ENSO amplitude. The  
25 multi-model mean ENSO amplitude increases by 17% with increased sulfate aerosols, with more El  
26 Niño and La Niña years in all the PDRMIP models used in this study. Changes in the Niño3.4 index are  
27 significantly correlated with changes in the EAWM index.

28

29 In coupled simulations, the aerosol-induced broad cooling alters the mean state over the tropical and  
30 equatorial Pacific, generating westerly anomalies over the central Pacific (peak in autumn) and warm  
31 SST anomalies over the eastern Pacific from autumn to winter, which are key factors in increasing  
32 ENSO amplitude. Using a diagnostic analysis, the contribution of two main processes, the Bjerknes  
33 feedback and zonal wind forcing is estimated. The zonal wind forcing is identified to strengthen from  
34 the baseline experiment to the SUL×10Asia experiment by 8%, while the strength of the Bjerknes  
35 feedback almost doesn't change. Therefore, the aerosol-induced cooling weakens the easterly trade  
36 winds over the central Pacific, which reduce the east-west equatorial Pacific SST gradient through the



1 zonal wind forcing, causing the increased amplitude of ENSO and the EAWM. In summary, the findings  
2 of this study provide a better understanding of the change to the year-to-year variability of the EAWM  
3 in response to aerosol forcing. This is critical to reducing uncertainties in future projections of  
4 variability of regional extremes, such as cold surges and flooding, which can cause large social and  
5 economic impacts on densely populated East Asia.

6

7 We acknowledge some limitations and potential extensions of this study. Only a limited number of  
8 models is available as part of PDRMIP, as some others do not parameterise aerosol-cloud interactions  
9 which are critical to realise the total aerosol response across Asia (e.g. Dong et al., 2016; Liu et al.,  
10 2024). Also, some models prescribed concentrations, rather than emissions, perturbations, the  
11 implications of which are difficult to ascertain given the limited model sample. Including more models  
12 and making use of coordinated perturbed aerosol experiments to Asian aerosols, such as those planned  
13 as part of RAMIP (Wilcox et al., 2023) would further increase the robustness of our study. This would  
14 allow to better characterise the individual model responses as a function of the underlying bias (e.g.,  
15 Liu et al., 2024). It would be interesting to extend this analysis to future projections for the 21<sup>st</sup> century,  
16 for example using CMIP6 models or large ensembles, and examine the externally-forced changes  
17 accounting also for the role of internal climate variability. It would also be interesting to examine the  
18 extent to which the ENSO-EAWM link varies across the various future aerosol pathways, which are  
19 uncertain and display very different, but equally plausible, patterns over Asia (Persad et al., 2022; Wang  
20 et al., 2023). Finally, we only considered the role of Asian aerosol changes. A more comprehensive  
21 analysis, should similar experiments be available, could also consider aerosols from other geographical  
22 regions, such as Europe and North America, which can also affect the Pacific and, via atmospheric  
23 teleconnections, East Asia (e.g. Dong et al., 2016; Liu et al., 2019).

24

25

26 **Code availability.** The python code generated in this study is available upon request (contact author).

27

28 **Data availability.** The CRU land temperature dataset is obtained from  
29 [https://crudata.uea.ac.uk/cru/data/hrg/cru\\_ts\\_4.07](https://crudata.uea.ac.uk/cru/data/hrg/cru_ts_4.07), while the HadISST sea surface temperature dataset  
30 can be found at <https://www.metoffice.gov.uk/hadobs/hadisst/>. The ERA5 reanalysis is provided by the  
31 European Centre for Medium-Range Weather Forecasts at  
32 <https://www.ecmwf.int/en/forecasts/dataset/ecmwf-reanalysis-v5>. The PDRMIP data can be accessed  
33 through the World Data Center for Climate (WDCC) data server at  
34 [https://doi.org/10.26050/WDCC/PDRMIP\\_2012-2021](https://doi.org/10.26050/WDCC/PDRMIP_2012-2021).

35

36 **Author contribution.** ZJ and MAB designed the study and discussed the results. ZJ carried out the  
37 analysis and drafted the manuscript. All authors edited the paper.



1

2 **Competing interests.** The authors have no competing interests to declare.

3

4 **Acknowledgements.** ZJ thanks the Startup Foundation for Introducing Talent of Nanjing University of  
5 Information Science and Technology (NUIST) (grant no. 2024r034) and Natural Science Fund for  
6 Colleges and Universities in Jiangsu Province (grant no. 24KJB170015). MB acknowledges support  
7 from the Natural Environment Research Council (grant no. NE/N006038/1) and the Research Council  
8 of Norway (grant no. 324182; CATHY).

## 9 **References**

- 10 Allen, R. J., Evan, A. T., Booth, B. B. B., Allen, R. J., Evan, A. T., and Booth, B. B. B.:  
11 Interhemispheric Aerosol Radiative Forcing and Tropical Precipitation Shifts during the Late  
12 Twentieth Century, *J. Climate*, 28, 8219–8246, <https://doi.org/10.1175/JCLI-D-15-0148.1>,  
13 2015.
- 14 Bellenger, H., Guilyardi, E., Leloup, J., Lengaigne, M., and Vialard, J.: ENSO representation in  
15 climate models: from CMIP3 to CMIP5, *Clim. Dyn.*, 42, 1999–2018,  
16 <https://doi.org/10.1007/s00382-013-1783-z>, 2014.
- 17 Bartlett, R.E., Bollasina, M.A., Booth, B.B., Dunstone, N.J., Marengo, F., Messori, G. and Bernie, D.J.:  
18 Do differences in future sulfate emission pathways matter for near-term climate? A case study  
19 for the Asian monsoon, *Clim. Dyn.*, 50, pp.1863-1880, <https://doi.org/10.1007/s00382-017-3726-6>, 2018.
- 21 Bollasina, M.A., Ming, Y. and Ramaswamy, V., et al.: Contribution of local and remote anthropogenic  
22 aerosols to the twentieth century weakening of the South Asian monsoon, *Geophys. Res. Lett.*,  
23 41(2), pp.680-687, <https://doi.org/10.1002/2013GL058183>, 2014.
- 24 Beobide-Arsuaga, G., Bayr, T., Reintges, A., & Latif, M.: Uncertainty of ENSO-amplitude projections  
25 in CMIP5 and CMIP6 models, *Clim. Dyn.* 56, pp.3875-3888, <https://doi.org/10.1007/s00382-021-05673-4>, 2021.
- 27 Boucher, O., Randall, D., Artaxo, P., Bretherton, C., Feingold, G., Forster, P., Kerminen, V.-M., Kondo,  
28 Y., Liao, H., Lohmann, U., Rasch, P., Satheesh, S., Sherwood, S., Stevens, B., and Zhang, X.:  
29 Clouds and Aerosols, in: *Climate Change 2013: The Physical Science Basis, Contribution of*  
30 *Working Group I to the Fifth Assessment Report of the Intergovernmental Panel on Climate*  
31 *Change*, chap. Clouds and, Cambridge University Press, Cambridge, United Kingdom and New  
32 York, NY, USA, 2013.
- 33 Cai, W., Borlace, S., Lengaigne, M., Van Rensch, P., Collins, M., Vecchi, G., Timmermann, A.,  
34 Santoso, A., McPhaden, M.J., Wu, L. and England, M.H.: Increasing frequency of extreme El



- 1 Niño events due to greenhouse warming, *Nature climate change*, 4(2), pp.111-116,  
2 <https://doi.org/10.1038/nclimate2100>, 2014.
- 3 Cai, W., Santoso, A., Collins, M., Dewitte, B., Karamperidou, C., Kug, J.S., Lengaigne, M., McPhaden,  
4 M.J., Stuecker, M.F., Taschetto, A.S. and Timmermann, A.: Changing El Niño–Southern  
5 oscillation in a warming climate, *Nature Reviews Earth & Environment*, 2(9), pp.628-644,  
6 <https://doi.org/10.1038/s43017-021-00199-z>, 2021.
- 7 Chang, C.P., Wang, Z. and Hendon, H.: *The Asian winter monsoon The Asian Monsoon* (Berlin:  
8 Springer Praxis Books), pp.89–127, 2006.
- 9 Chen, W., Yang, S. and Huang, R.H.: Relationship between stationary planetary wave activity and the  
10 East Asian winter monsoon, *Journal of Geophysical Research: Atmospheres*, 110(D14),  
11 <https://doi.org/10.1029/2004JD005669>, 2005.
- 12 Chen, W., Wang, L., Feng, J., Wen, Z., Ma, T., Yang, X., & Wang, C.: Recent progress in studies of  
13 the variabilities and mechanisms of the East Asian monsoon in a changing climate, *Advances*  
14 *in Atmospheric Sciences*, 36(9), 887–901, <https://doi.org/10.1007/s00376-019-8230-y>, 2019.
- 15 Cheng, J., Su, J., Cui, T., Li, X., Dong, X., Sun, F., Yang, Y., Tong, D., Zheng, Y., Li, Y. and Li, J.:  
16 Dominant role of emission reduction in PM<sub>2.5</sub> air quality improvement in Beijing during 2013–  
17 2017: a model-based decomposition analysis, *Atmospheric Chemistry and Physics*, 19(9),  
18 6125-6146, <https://doi.org/10.5194/acp-19-6125-2019>, 2019.
- 19 Collins, M., An, S.I., Cai, W., Ganachaud, A., Guilyardi, E., Jin, F.F., Jochum, M., Lengaigne, M.,  
20 Power, S., Timmermann, A. and Vecchi, G.: The impact of global warming on the tropical  
21 Pacific Ocean and El Niño, *Nature Geoscience*, 3(6), pp.391-397,  
22 <https://doi.org/10.1038/ngeo868>, 2010.
- 23 Copernicus Climate Change Service (C3S): ERA5: fifth genera- tion of ECMWF atmospheric  
24 reanalyses of the global climate, Copernicus Climate Change Service Climate Data Store (CDS)  
25 [data set], 15(2), 2020, <https://cds.climate.copernicus.eu/cdsapp#!home> (last access: 16 May  
26 2022), 2017.
- 27 Dong, B., Sutton, R. T., Highwood, E. J., and Wilcox, L. J.: Preferred response of the East Asian  
28 summer monsoon to local and non-local anthropogenic sulphur dioxide emissions, *Clim. Dyn.*,  
29 <https://doi.org/10.1007/s00382-015-6782-6>, 2016.
- 30 Dow, W. J., Maycock, A. C., Lofverstrom, M., & Smith, C. J.: The effect of anthropogenic aerosols on  
31 the Aleutian low, *J. Climate*, 34(5), 1725-1741, <https://doi.org/10.1175/JCLI-D-20-0423.1>,  
32 2021.
- 33 Fahrenbach, N.L., Bollasina, M.A., Samset, B.H., Cowan, T. and Ekman, A.M.: Asian Anthropogenic  
34 Aerosol Forcing Played a Key Role in the Multidecadal Increase in Australian Summer  
35 Monsoon Rainfall, *J. Climate*, 37(3), pp.895-911, <https://doi.org/10.1175/JCLI-D-23-0313.1>,  
36 2024.



- 1 Feng, J., L. Wang, W. Chen, S. K. Fong, and K. C. Leong: Different impacts of two types of Pacific  
2 Ocean warming on Southeast Asian rainfall during boreal winter, *J. Geophys. Res.*, 115,  
3 D24122, <https://doi.org/10.1029/2010JD014761>, 2010.
- 4 Forster, P., Storelvmo, T., Armour, K., Collins, W., Dufresne, J. L., Frame, D., Lunt, D. J., Mauritsen,  
5 T., Palmer, M. D., Watanabe, M., Wild, M., and Zhang, H.: The Earth's Energy Budget, Cli-  
6 mate Feedbacks, and Climate Sensitivity, in: *Climate Change 2021: The Physical Science*  
7 *Basis, Contribution of Working Group I to the Sixth Assessment Report of the*  
8 *Intergovernmental Panel on Climate Change*, Cambridge University Press, 2021.
- 9 Gao, J., Wang, K., Wang, Y., Liu, S., Zhu, C., Hao, J., Liu, H., Hua, S. and Tian, H.: Temporal-spatial  
10 characteristics and source apportionment of PM<sub>2.5</sub> as well as its associated chemical species  
11 in the Beijing-Tianjin-Hebei region of China, *Environmental pollution*, 233, pp.714-724,  
12 <https://doi.org/10.1016/j.envpol.2017.10.123>, 2018.
- 13 Gong, H., L. Wang, W. Chen, R. Wu, K. Wei, and X. Cui: The Climatology and Interannual Variability  
14 of the East Asian Winter Monsoon in CMIP5 Models. *J. Climate*, 27, 1659–1678,  
15 <https://doi.org/10.1175/JCLI-D-13-00039.1>, 2014.
- 16 Gong, H., Wang, L., Chen, W., Nath, D., Huang, G. and Tao, W.: Diverse influences of ENSO on the  
17 East Asian–Western Pacific winter climate tied to different ENSO properties in CMIP5 models  
18 *J. Clim.* 28 2187–202, <https://doi.org/10.1175/JCLI-D-14-00405.1>, 2015.
- 19 Harris, I., Osborn, T. J., Jones, P. and Lister, D.: Version 4 of the CRU TS monthly high-resolution  
20 gridded multivariate climate dataset *Sci. Data* 7, 2020.
- 21 Hayashi, M., Jin, F. F. & Stuecker, M. F. Dynamics for El Niño-La Niña asymmetry constrain  
22 equatorial-Pacific warming pattern, *Nat. Commun.*, 11, 4230, [https://doi.org/10.1038/s41467-](https://doi.org/10.1038/s41467-020-17983-y)  
23 [020-17983-y](https://doi.org/10.1038/s41467-020-17983-y), 2020.
- 24 He, S., Wang, H., & Liu, J.: Changes in the Relationship between ENSO and Asia–Pacific Midlatitude  
25 Winter Atmospheric Circulation. 26(10), 3377-3393. [https://dx.doi.org/10.1175/JCLI-D-12-](https://dx.doi.org/10.1175/JCLI-D-12-00355.1)  
26 [00355.1](https://dx.doi.org/10.1175/JCLI-D-12-00355.1), 2013.
- 27 Hersbach, H., Bell, B., Berrisford, P., Biavati, G., Horányi, A., Muñoz Sabater, J., Nicolas, J., Peubey,  
28 C., Radu, R., Rozum, I., Schepers, D., Simmons, A., Soci, C., Dee, D., Thépaut, J-N: ERA5  
29 monthly averaged data on pressure levels from 1940 to present. Copernicus Climate Change  
30 Service (C3S) Climate Data Store (CDS), DOI: 10.24381/cds.6860a573 (Accessed on DD-  
31 MMM-YYYY), 2023.
- 32 Hu, C., Yang, S., & Wu, Q.: An optimal index for measuring the effect of East Asian winter monsoon  
33 on China winter temperature, *Climate Dynamics*, 45(9–10), 2571–2589,  
34 <https://doi.org/10.1007/s00382-015-2493-5>, 2015.
- 35 Huang, R., Chen, J., Wang, L., & Lin, Z.: Characteristics, processes, and causes of the spatio-temporal  
36 variabilities of the East Asian monsoon system, *Advances in Atmospheric Sciences*, 29(5),  
37 910–942, <https://doi.org/10.1007/s00376-012-2015-x>, 2012.



- 1 Huang, P., & Xie, S. P.: Mechanisms of change in ENSO-induced tropical Pacific rainfall variability in  
2 a warming climate, *Nature Geoscience*, 8(12), pp.922-926, <https://doi.org/10.1038/ngeo2571>,  
3 2015.
- 4 Huang, B. et al: Extended reconstructed sea surface temperature, version 5 (ERSSTv5): upgrades,  
5 validations, and intercomparisons. *J. Clim.* 30, 8179–8205, [https://doi.org/10.1175/JCLI-D-](https://doi.org/10.1175/JCLI-D-16-0836.1)  
6 16-0836.1, 2017.
- 7 Hwang, Y.-T., Frierson, D. M. W., and Kang, S. M.: Anthropogenic sulfate aerosol and the southward  
8 shift of tropical precipitation in the late 20th century, *Geophys. Res. Lett.*, 40, 2845–2850,  
9 <https://doi.org/10.1002/grl.50502>, 2013.
- 10 Ji, L., Sun, S., Arpe, K. and Bengtsson, L.: Model study on the interannual variability of Asian winter  
11 monsoon and its influence, *Adv. Atmos. Sci.*, 14, 1–22, [https://doi.org/10.1007/s00376-997-](https://doi.org/10.1007/s00376-997-0039-4)  
12 0039-4, 1997.
- 13 Jia, Z., Bollasina, M.A., Li, C., Doherty, R. and Wild, O.: Changes in the relationship between ENSO  
14 and the East Asian winter monsoon under global warming, *Environ. Res. Lett.*, 15(12),  
15 p.124056, <https://doi.org/10.1088/1748-9326/abca63>, 2020.
- 16 Jin, F. F.: An equatorial ocean recharge paradigm for ENSO. Part II: A stripped-down coupled  
17 model. *Journal of the Atmospheric Sciences*, 54(7), 830-847, [https://doi.org/10.1175/1520-](https://doi.org/10.1175/1520-0469(1997)054<0830:AEORPF>2.0.CO;2)  
18 0469(1997)054<0830:AEORPF>2.0.CO;2, 1997.
- 19 Jin, F., and An, S.: Thermocline and zonal advective feedbacks within the equatorial ocean recharge  
20 oscillator model for ENSO, *Geophys. Res. Lett.* 26, 2989–2992,  
21 <https://doi.org/10.1029/1999GL002297>, 1999.
- 22 Jiang, Y., Yang, X.Q., Liu, X., Yang, D., Sun, X., Wang, M., Ding, A., Wang, T. and Fu, C.:  
23 Anthropogenic aerosol effects on East Asian winter monsoon: The role of black carbon-induced  
24 Tibetan Plateau warming, *Journal of Geophysical Research: Atmospheres*, 122(11), pp.5883-  
25 5902, <https://doi.org/10.1002/2016JD026237>, 2017.
- 26 Jiang, W., Gong, H., Huang, P., Wang, L., Huang, G. and Hu, L.: Biases and improvements of the  
27 ENSO-East Asian winter monsoon teleconnection in CMIP5 and CMIP6 models, *Climate*  
28 *Dynamics*, 59(7), pp.2467-2480, <https://doi.org/10.1007/s00382-022-06220-5>, 2022.
- 29 Kim, S. T., Cai, W., Jin, F. F., and Yu, J. Y.: ENSO stability in coupled climate models and its  
30 association with mean state, *Clim. Dyn.*, 42, 3313–3321, [https://doi.org/10.1007/s00382-013-](https://doi.org/10.1007/s00382-013-1833-6)  
31 1833-6, 2014.
- 32 Kobayashi, S., Ota, Y., Harada, Y., Ebata, A., Moriya, M., Onoda, H., Onogi, K., Kamahori, H.,  
33 Kobayashi, C., Endo, H. and Miyaoka, K.: The JRA-55 reanalysis: General specifications and  
34 basic characteristics, *Journal of the Meteorological Society of Japan, Ser. II*, 93(1), pp.5-48,  
35 <https://doi.org/10.2151/jmsj.2015-001>, 2015.





- 1 Lewinschal, A., Ekman, A. M. L., and Körnich, H.: The role of precipitation in aerosol-induced changes  
2 in northern hemisphere wintertime stationary waves, *Clim. Dynam.*, 41, 647–661,  
3 <https://doi.org/10.1007/s00382-012-1622-7>, 2013.
- 4 Li, F., & Wang, H.: Autumn sea ice cover, winter Northern Hemisphere annular mode, and winter  
5 precipitation in Eurasia, *Journal of Climate*, 26(11), 3968–3981, [https://doi.org/10.1175/JCLI-](https://doi.org/10.1175/JCLI-D-12-00380.1)  
6 [D-12-00380.1](https://doi.org/10.1175/JCLI-D-12-00380.1), 2012.
- 7 Li, J., Carlson, B.E., Yung, Y.L., Lv, D., Hansen, J., Penner, J.E., Liao, H., Ramaswamy, V., Kahn,  
8 R.A., Zhang, P. and Dubovik, O.: Scattering and absorbing aerosols in the climate  
9 system, *Nature Reviews Earth & Environment*, 3(6), pp.363–379,  
10 <https://doi.org/10.1038/s43017-022-00296-7>, 2022.
- 11 Liao, H., Chang, W.Y., Yang, Y.: Climatic effects of air pollutants over China: A review, *Advances in*  
12 *Atmospheric Sciences*, 32(1), pp.115–139, <https://doi.org/10.1007/s00376-014-0013-x>, 2015.
- 13 Lian, T., Chen, D., Ying, J., Huang, P. & Tang, Y.: Tropical Pacific trends under global warming: El  
14 Niño-like or La Niña-like? *Natl Sci. Rev.*, 5, 810–812, <https://doi.org/10.1093/nsr/nwy134>,  
15 2018.
- 16 Lian, T., Chen, D.: The essential role of early-spring westerly wind burst in generating the centennial  
17 extreme 1997/98 El Niño, *J. Clim.*, 1:1–38, <https://doi.org/10.1175/JCLI-D-21-0010.1>, 2021.
- 18 Liu, Y., Sun, J. R., Yang, B.: The effects of black carbon and sulphate aerosols in China regions on East  
19 Asia monsoons, *Tellus B: Chemical and Physical Meteorology*, 61(4): 642–656,  
20 <https://doi.org/10.1111/j.1600-0889.2009.00427.x>, 2009.
- 21 Liu, L., Shawki, D., Voulgarakis, A., Kasoar, M., Samset, B.H., Myhre, G., Forster, P.M., Hodnebrog,  
22 Ø., Sillmann, J., Aalbergjø, S.G. and Boucher, O.: A PDRMIP multimodel study on the  
23 impacts of regional aerosol forcings on global and regional precipitation, *Journal of*  
24 *climate*, 31(11), pp.4429–4447, <https://doi.org/10.1175/JCLI-D-17-0439.1>, 2018.
- 25 Liu, Z., Ming, Y., Wang, L., Bollasina, M., Luo, M., Lau, N.C. and Yim, S.H.L.: A model investigation  
26 of aerosol-induced changes in the east Asian winter monsoon, *Geophysical research*  
27 *letters*, 46(16), pp.10186–10195, <https://doi.org/10.1029/2019GL084228>, 2019.
- 28 Liu, Z., Bollasina, M., and Wilcox, L.: Impact of Asian aerosols on the summer monsoon strongly  
29 modulated by regional precipitation biases, *EGUsphere [preprint]*,  
30 <https://doi.org/10.5194/egusphere-2023-3136>, 2024.
- 31 McPhaden, M. J.: Genesis and evolution of the 1997–98 El Nino. *Science* 283:950–954.  
32 <https://doi.org/10.1126/science.283.5404.950>, 1999.
- 33 Myhre, G., Shindell, D., Bréon, F.-M., Collins, W., Fuglestedt, J., Huang, J., Koch, D., Lamarque, J.-  
34 F., Lee, D., Mendoza, B., Nakajima, T., Robock, A., Stephens, G., Takemura, T., and Zhang,  
35 H.: Anthropogenic and Natural Radiative Forcing, in: *Climate Change 2013, The Physical*  
36 *Science Basis, Contribution of Working Group I to the Fifth Assessment Report of the Inter-*  
37 *governmental Panel on Climate Change*, edited by: Stocker, T. F., Qin, D., Plattner, G.-K.,



- 1 Tignor, M., Allen, S. K., Boschung, J., Nauels, A., Xia, Y., Bex, V., and Midgley, P. M.,  
2 Cambridge University Press, Cambridge, United Kingdom and New York, NY, USA, 2013.
- 3 Myhre, G., Forster, P.M., Samset, B.H., Hodnebrog, Ø., Sillmann, J., Aalbergsjø, S.G., Andrews, T.,  
4 Boucher, O., Faluvegi, G., Fläschner, D. and Iversen, T.: PDRMIP: A precipitation driver and  
5 response model intercomparison project—Protocol and preliminary results, *Bulletin of the*  
6 *American Meteorological Society*, 98(6), pp.1185-1198, [https://doi.org/10.1175/BAMS-D-16-](https://doi.org/10.1175/BAMS-D-16-0019.1)  
7 0019.1, 2017.
- 8 Navarro, J. C. A., Ekman, A. M. L., Pausata, F. S. R., Lewinschal, A., Varma, V., Seland, Ø., Gauss,  
9 M., Iversen, T., Kirkevåg, A., Riipinen, I., and Hansson, H. C.: Future Response of Temperature  
10 and Precipitation to Reduced Aerosol Emissions as Compared with Increased Greenhouse Gas  
11 Concentrations, *J. Climate*, 30, 939–954, <https://doi.org/10.1175/JCLI-D-16-0466.1>, 2017.
- 12 Persad, G.G., Samset, B.H. and Wilcox, L.J.: Aerosols must be included in climate risk  
13 assessments. *Nature*, 611(7937), pp.662-664, <https://doi.org/10.1038/d41586-022-03763-9>,  
14 2022.
- 15 Persad, G. G.: The dependence of aerosols' global and local precipitation impacts on the emitting  
16 region, *Atmos. Chem. Phys.*, 23, 3435–3452, <https://doi.org/10.5194/acp-23-3435-2023>, 2023.
- 17 Power, S., Delage, F., Chung, C., Kociuba, G. and Keay, K.: Robust twenty-first-century projections of  
18 El Niño and related precipitation variability, *Nature*, 502(7472), pp.541-545,  
19 <https://doi.org/10.1038/nature12580>, 2013.
- 20 Rayner, N. A., Parker, D. E., Horton, E. B., Folland, C. K., Alexander, L. V., & Rowell, D. P.: Global  
21 analyses of sea surface temperature, sea ice, and night marine air temperature since the late  
22 nineteenth century, *Journal of Geophysical Research*, 108, 4407.  
23 <https://doi.org/10.1029/2002JD002670>, 2003.
- 24 Ramanathan, V., Chung, C., Kim, D., Bettge, T., Buja, L., Kiehl, J. T., Washington, W. M., Fu, Q.,  
25 Sikka, D. R., and Wild, M.: Atmospheric brown clouds: impacts on South Asian climate and  
26 hydrological cycle, *P. Natl. Acad. Sci. USA*, 102, 5326–5333,  
27 <https://doi.org/10.1073/pnas.0500656102>, 2005.
- 28 Rashid, H. A., Hirst, A. C., and Marsland, S. J.: An atmospheric mechanism for ENSO amplitude  
29 changes under an abrupt quadrupling of CO<sub>2</sub> concentration in CMIP5 models, *Geophys. Res.*  
30 *Let.*, 43, 1687–1694, <https://doi.org/10.1002/2015GL066768>, 2016.
- 31 Rashid, H. A.: Forced changes in El Niño–Southern Oscillation due to global warming and the  
32 associated uncertainties in ACCESS-ESM1.5 large ensembles, *Front. Clim.*, 4:954449,  
33 <https://doi.org/10.3389/fclim.2022.954449>, 2022.
- 34 Rotstayn, L. D., and Lohmann, U.: Tropical Rainfall Trends and the Indirect Aerosol Effect, *J. Climate*,  
35 15, 2103–2116, [https://doi.org/10.1175/1520-0442\(2002\)015<2103:TRTATI>2.0.CO;2](https://doi.org/10.1175/1520-0442(2002)015<2103:TRTATI>2.0.CO;2), 2002.



- 1 Shindell, D. T., Voulgarakis, A., Faluvegi, G., and Milly, G.: Precipitation response to regional radiative  
2 forcing, *Atmos. Chem. Phys.*, 12, 6969–6982, <https://doi.org/10.5194/acp-12-6969-2012>,  
3 2012.
- 4 Song, F.F., Zhou, T.T., Qian, Y.: Responses of East Asian summer monsoon to natural and  
5 anthropogenic forcings in the 17 latest CMIP5 models, *Geophysical Research Letters*, 41(2),  
6 pp.596-603, <https://doi.org/10.1002/2013GL058705>, 2014.
- 7 Timmermann, A., An, S.I., Kug, J.S., Jin, F.F., Cai, W., Capotondi, A., Cobb, K.M., Lengaigne, M.,  
8 McPhaden, M.J., Stuecker, M.F. and Stein, K.: El Niño–southern oscillation  
9 complexity, *Nature*, 559(7715), pp.535-545, <https://doi.org/10.1038/s41586-018-0252-6>,  
10 2018.
- 11 Vecchi, G.A., Soden, B.J., Wittenberg, A.T., Held, I.M., Leetmaa, A. and Harrison, M.J.: Weakening  
12 of tropical Pacific atmospheric circulation due to anthropogenic forcing, *Nature*, 441(7089),  
13 pp.73-76, <https://doi.org/10.1038/nature04744>, 2006.
- 14 Voigt, A., Pincus, R., Stevens, B., Bony, S., Boucher, O., Bellouin, N., Lewinschal, A., Medeiros, B.,  
15 Wang, Z., and Zhang, H.: Fast and slow shifts of the zonal-mean intertropical convergence zone  
16 in response to an idealized anthropogenic aerosol, *J. Adv. Model. Earth Sy.*, 9, 870–892,  
17 <https://doi.org/10.1002/2016MS000902>, 2017.
- 18 Wang, B., Wu, R., & Fu, X.: Pacific–East Asian teleconnection: how does ENSO affect East Asian  
19 climate? *Journal of Climate*, 13(9), 1517-1536, [https://doi.org/10.1175/1520-0442\(2000\)013<1517:PEATHD>2.0.CO;2](https://doi.org/10.1175/1520-0442(2000)013<1517:PEATHD>2.0.CO;2), 2000.
- 21 Wang, F. K.: Confidence interval for the mean of non-normal data, *Qual. Reliab. Eng. Int.*, 17, 257–  
22 267, <https://doi.org/10.1002/qre.400>, 2001.
- 23 Wang, B., An, S.A.: Mechanism for decadal changes of ENSO behavior: Roles of background wind  
24 changes, *Clim Dyn*, 18, pp.475–486, <https://doi.org/10.1007/s00382-001-0189-5>, 2002.
- 25 Wang, Z. Wu, C.-P. Chang, J. Liu, J. Li, and T. Zhou: Another look at interannual-to-interdecadal  
26 variations of the East Asian winter monsoon: The northern and southern temperature modes, *J.*  
27 *Climate*, 23, 1495–1512, <https://doi.org/10.1175/2009JCLI3243.1>, 2010.
- 28 Wang, H., He, S., & Liu, J.: Present and future relationship between the East Asian winter monsoon  
29 and ENSO: Results of CMIP5, *Journal of Geophysical Research: Oceans*, 118(10), 5222-5237,  
30 <https://doi.org/10.1002/jgrc.20332>, 2013.
- 31 Wang, G., Cai, W., Gan, B., Wu, L., Santoso, A., Lin, X., Chen, Z. and McPhaden, M.J.: Continued  
32 increase of extreme El Niño frequency long after 1.5 C warming stabilization, *Nature Climate*  
33 *Change*, 7(8), pp.568-572, <https://doi.org/10.1038/nclimate3351>, 2017.
- 34 Wang, Z., Wu, R., Gong, H., Jia, X., & Dai, P.: What determine the performance of the ENSO-East  
35 Asian winter monsoon relationship in CMIP6 models? *Journal of Geophysical Research:*  
36 *Atmospheres*, 127, e2021JD036227, <https://doi.org/10.1029/2021JD036227>, 2022.



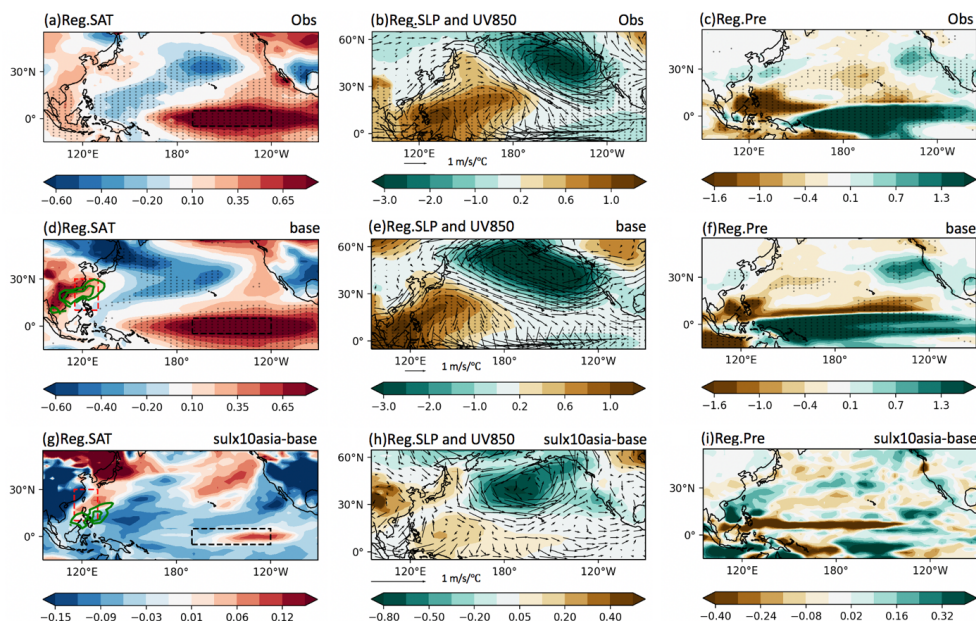
- 1 Wang, P., Yang, Y., Xue, D., Ren, L., Tang, J., Leung, L. R., & Liao, H.: Aerosols overtake greenhouse  
2 gases causing a warmer climate and more weather extremes toward carbon neutrality, *Nature*  
3 *Communications*, 14(1), 7257, <https://doi.org/10.1038/s41467-023-42891-2>, 2023.
- 4 Westervelt, D. M., Conley, A. J., Fiore, A. M., Lamarque, J.-F., Shindell, D. T., Previdi, M., Mascioli,  
5 N. R., Faluvegi, G., Correa, G., and Horowitz, L. W.: Connecting regional aerosol emissions  
6 reductions to local and remote precipitation responses, *Atmos. Chem. Phys.*, 18, 12461–12475,  
7 <https://doi.org/10.5194/acp-18-12461-2018>, 2018.
- 8 Westervelt, D. M., Mascioli, N. R., Fiore, A. M., Conley, A. J., Lamarque, J.-F., Shindell, D. T.,  
9 Faluvegi, G., Previdi, M., Correa, G., and Horowitz, L. W.: Local and remote mean and extreme  
10 temperature response to regional aerosol emissions reductions, *Atmos. Chem. Phys.*, 20, 3009–  
11 3027, <https://doi.org/10.5194/acp-20-3009-2020>, 2020.
- 12 Wilcox, L. J., Dunstone, N., Lewinschal, A., Bollasina, M., Ekman, A. M. L., and Highwood, E. J.:  
13 Mechanisms for a remote response to Asian anthropogenic aerosol in boreal winter, *Atmos.*  
14 *Chem. Phys.*, 19, 9081–9095, <https://doi.org/10.5194/acp-19-9081-2019>, 2019.
- 15 Wilcox, L. J., Allen, R. J., Samset, B. H., Bollasina, M. A., Griffiths, P. T., Keeble, J., Lund, M. T.,  
16 Makkonen, R., Merikanto, J., O'Donnell, D., Paynter, D. J., Persad, G. G., Rumbold, S. T.,  
17 Takemura, T., Tsigaridis, K., Undorf, S., and Westervelt, D. M.: The Regional Aerosol Model  
18 Intercomparison Project (RAMIP), *Geosci. Model Dev.*, 16, 4451–4479,  
19 <https://doi.org/10.5194/gmd-16-4451-2023>, 2023.
- 20 Xuan, Z., Zhang, W., Jiang, F., Stuecker, M.F. and Jin, F.F.: Seasonal-varying characteristics of tropical  
21 Pacific westerly wind bursts during El Niño due to annual cycle modulation, *Climate*  
22 *Dynamics*, 62(1), pp.299-314, <https://doi.org/10.1007/s00382-023-06907-3>, 2024.
- 23 Yan, Z., Wu, B., Li, T., Collins, M., Clark, R., Zhou, T., Murphy, J. and Tan, G.: Eastward shift and  
24 extension of ENSO-induced tropical precipitation anomalies under global warming, *science*  
25 *advances*, 6(2), p.eaax4177, <https://doi.org/10.1126/sciadv.aax4177>, 2020
- 26 Yang, S., Lau, K.-M., & Kim, K.-M.: Variations of the East Asian jet stream and Asian–Pacific–  
27 American winter climate anomalies, *Journal of Climate*, 15(3), 306–325,  
28 [https://doi.org/10.1175/1520-0442\(2002\)015<0306:VOTEAJ>2.0.CO;2](https://doi.org/10.1175/1520-0442(2002)015<0306:VOTEAJ>2.0.CO;2), 2002.
- 29 Ying, J., Huang, P., Lian, T. & Chen, D.: Intermodel uncertainty in the change of ENSO's amplitude  
30 under global warming: role of the response of atmospheric circulation to SST anomalies, *J.*  
31 *Clim.* 32, 369–383, <https://doi.org/10.1175/JCLI-D-18-0456.1>, 2019.
- 32 Zhang, R., Sumi, A. and Kimoto, M.: Impact of El Niño on the East Asian monsoon a diagnostic study  
33 of the '86/87 and '91/92 events, *Journal of the Meteorological Society of Japan. Ser. II*, 74(1),  
34 pp.49-62, [https://doi.org/10.2151/jmsj1965.74.1\\_49](https://doi.org/10.2151/jmsj1965.74.1_49), 1996.
- 35 Zhang, H., Chen, S., Zhong, J., Zhang, S., Zhang, Y., Zhang, X., Li, Z. and Zeng, X.C.: Formation of  
36 aqueous-phase sulfate during the haze period in China: Kinetics and atmospheric implications,



- 1           Atmospheric Environment, 177, pp.93-99, <https://doi.org/10.1016/j.atmosenv.2018.01.017>,  
2           2018.  
3  
4   Zhao, S. and Suzuki, K.: Differing impacts of black carbon and sulfate aerosols on global precipitation  
5           and the ITCZ location via atmosphere and ocean energy perturbations, Journal of  
6           Climate, 32(17), pp.5567-5582, <https://doi.org/10.1175/JCLI-D-18-0616.1>, 2019.  
7   Zheng, X.-T., Xie, S.-P., Lv, L. H. & Zhou, Z. Q.: Intermodel uncertainty in ENSO amplitude change  
8           tied to Pacific Ocean warming pattern, J. Clim. 29, 7265–7279, [https://doi.org/10.1175/JCLI-](https://doi.org/10.1175/JCLI-D-16-0039.1)  
9           D-16-0039.1, 2016.  
10   Zhou, B., Gu, L., Ding, Y., Shao, L., Wu, Z., Yang, X., Li, C., Li, Z., Wang, X., Cao, Y. and Zeng,  
11           B.: The great 2008 Chinese ice storm: its socioeconomic–ecological impact and sustainability  
12           lessons learned, Bulletin of the American meteorological Society, 92(1), pp.47-60,  
13           <https://doi.org/10.1175/2010BAMS2857.1>, 2011.  
14  
15  
16  
17



1 **Figures**



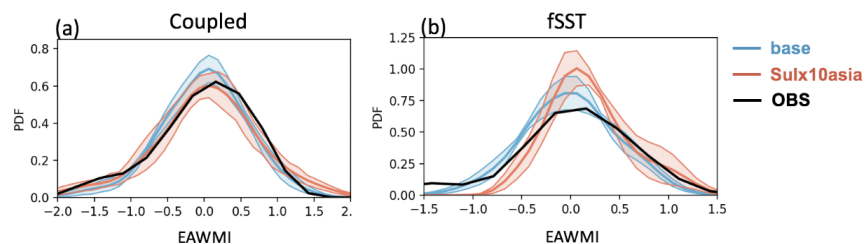
2

3 **Figure 1.** DJF regressions of (a)(d) surface air temperature (SAT, SST over the ocean, °C, shading) and 1000 hPa  
 4 meridional wind (V1000) over the broad East Asia (green contours, values plotted only when larger than 0.1 m  
 5  $s^{-1} \text{ } ^\circ\text{C}^{-1}$ ), (b)(e) sea level pressure (SLP; hPa, shading) and 850 hPa wind (UV850;  $m \text{ s}^{-1}$ , vector), (c)(f)  
 6 precipitation (Pre,  $mm \text{ d}^{-1}$ ) onto the Niño3.4 index from coupled (a-c) observations during 1965-2014, (d-f)  
 7 multimodel mean coupled baseline simulations in PDRMIP. Dotted regions indicate significant correlations at the  
 8 95% level from the two-tailed Student's  $t$  test. Differences in regressions of (g) SAT and V1000 (green contours,  
 9 values plotted only when larger than  $0.05 \text{ m s}^{-1} \text{ } ^\circ\text{C}^{-1}$ ), (h) SLP and UV850, (i) Pre between coupled SUL×10Asia  
 10 and baseline simulations. The definition regions of the EAWM index and the Niño3.4 index are marked by red  
 11 and black rectangles respectively.

12  
 13  
 14  
 15  
 16  
 17  
 18  
 19  
 20  
 21  
 22  
 23



1



2

3 **Figure 2.** Frequency distributions of the EAWM index from (a) observations during DJF 1965-2014 (black curve)  
4 and coupled simulations, (b) observations during DJF 1994-2005 (black curve) and fsST simulations in PDRMIP  
5 with multimodel-means (thick coloured curves) and the associated 95% confidence intervals (coloured shades).  
6 The confidence intervals are estimated from different models by using bootstrap resampling (e.g. Wang, 2001).

7

8

9

10

11

12

13

14

15

16

17

18

19

20

21

22

23

24

25

26

27

28

29

30

31

32

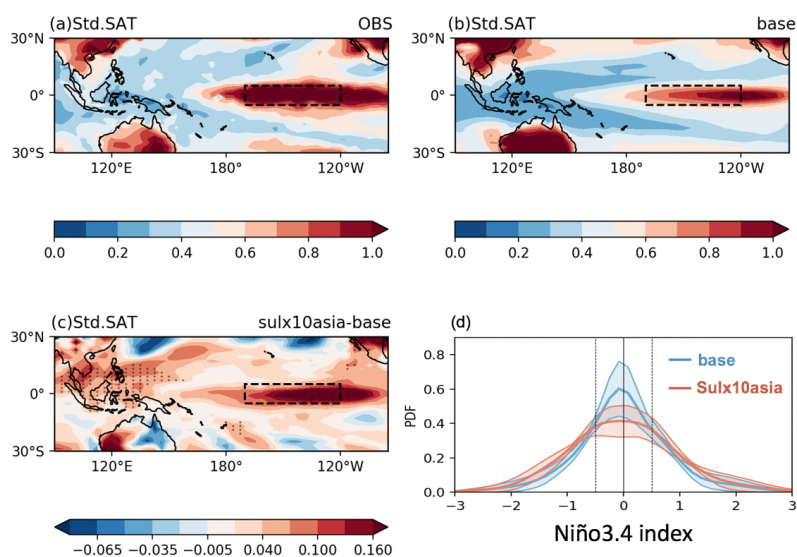
33

34





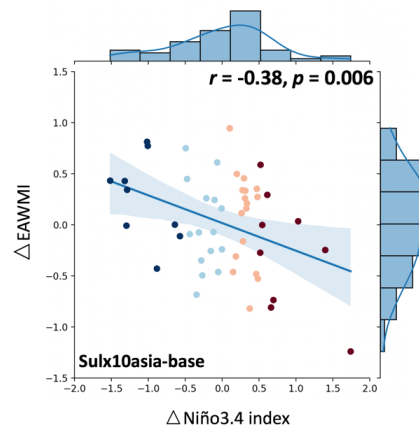
1



2

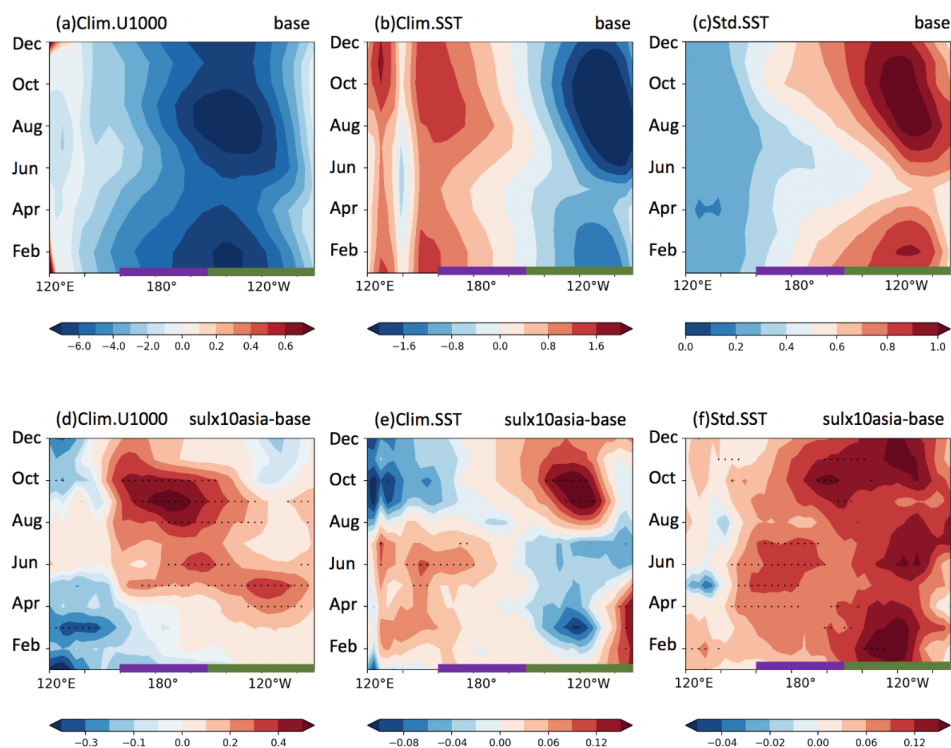
3 **Figure 3.** DJF multimodel mean standard deviations of SAT (SST over the ocean, °C) from (a) observations  
4 during 1965-2014, (b) coupled baseline simulations. (c) Differences in standard deviations of SAT (SST over the  
5 ocean, °C) between coupled SULx10Asia and baseline simulations. Dotted regions indicate significant  
6 differences at the 95% level from the two-tailed  $F$ -test. (d) Frequency distributions of the Niño3.4 index from  
7 coupled simulations in PDRMIP with multimodel-means (thick coloured curves) and the associated 95%  
8 confidence intervals (coloured shades). The confidence intervals are estimated from different models by using  
9 bootstrap resampling.

10  
11  
12  
13  
14  
15  
16  
17  
18  
19  
20  
21  
22



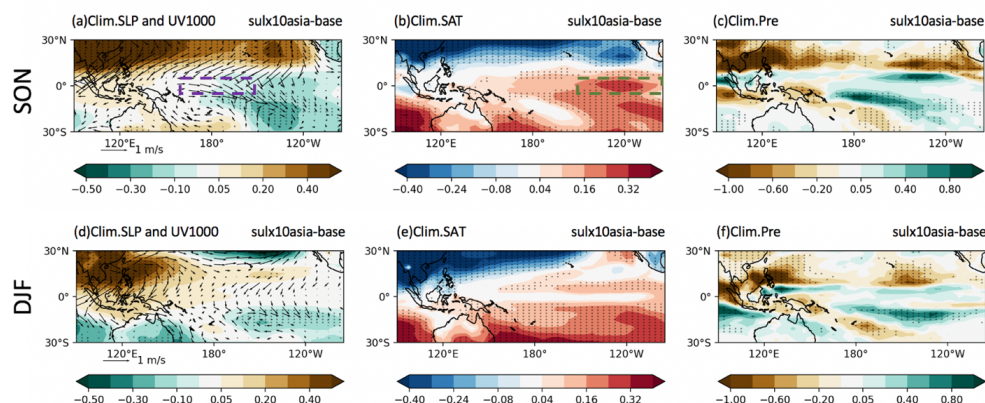
1  
2 **Figure 4.** Joint distributions of multimodel mean differences in the EAWM index against corresponding  
3 differences in the Niño3.4 index between coupled SUL×10Asia and baseline simulations, including the linear fits  
4 with 95% confidence intervals.

5  
6  
7  
8  
9  
10  
11  
12  
13  
14  
15  
16  
17  
18  
19  
20  
21  
22  
23  
24  
25  
26  
27  
28  
29



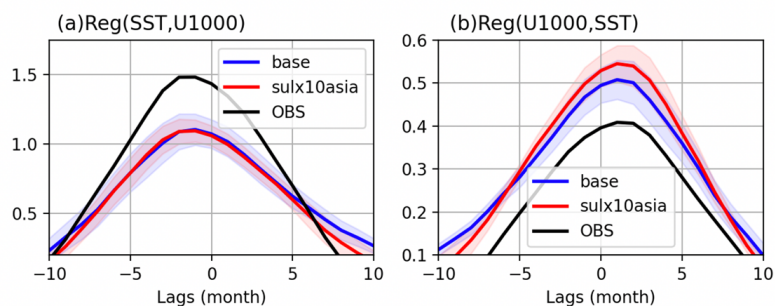
1  
 2 **Figure 5.** Multimodel mean longitudinal transect of the monthly climatological (a) 1000 hPa zonal wind (U1000,  
 3  $m s^{-1}$ ), (b) SST minus zonal mean ( $^{\circ}C$ ), (c) SST standard deviation ( $^{\circ}C$ ) for the equatorial Pacific ( $5^{\circ}S-5^{\circ}N$ ) from  
 4 coupled baseline simulations; and their changes in (d) U1000, (e) SST, (f) SST standard deviation between  
 5 coupled SUL $\times$ 10Asia and baseline simulations. Dotted regions in (d)(e) indicate significant changes at the 95%  
 6 level from the two-tailed Student's  $t$  test; in (f) indicate significant changes at the 95% level from the two-tailed  
 7  $F$ -test. The definition longitudes of the Niño3 and Niño4 indices are marked by green and purple thick bars  
 8 respectively along the x axis.

9  
 10  
 11  
 12  
 13  
 14  
 15  
 16  
 17  
 18  
 19



1  
2 **Figure 6.** (a-c) SON, (d-f) DJF multimodel mean changes in (a)(d) sea level pressure (SLP; hPa, shading) and  
3 1000 hPa wind (UV1000, vector), (b)(e) surface air temperature (SAT, SST over the ocean) minus domain mean  
4 ( $^{\circ}\text{C}$ ), (c)(f) precipitation (Pre,  $\text{mm d}^{-1}$ ) between coupled SUL $\times$ 10Asia and baseline simulations. Dotted regions  
5 indicate significant changes at the 95% level from the two-tailed Student's  $t$  test. The definition regions of the  
6 Niño3 and Niño4 indices are marked by green and purple rectangles in panels a-b respectively.

7  
8  
9  
10  
11  
12  
13  
14  
15  
16  
17  
18  
19  
20  
21  
22



1  
2 **Figure 7.** Multimodel mean lag-regression coefficients of (a) the Niño4 U1000 index onto the Niño3 SST index  
3 (indicative of the Bjerknes feedback) ( $\text{m s}^{-1} \text{ } ^\circ\text{C}^{-1}$ ), (b) the Niño3 SST index onto the Niño4 U1000 index  
4 (indicative of the zonal wind forcing of SST) ( $^\circ\text{C m}^{-1} \text{ s}$ ) from observations (black curve) and coupled simulations  
5 in PDRMIP with multimodel-means (thick coloured curves) and the associated 95% confidence intervals  
6 (coloured shades). The confidence intervals are estimated from different models by using bootstrap resampling.

7  
8  
9  
10  
11  
12  
13  
14  
15  
16  
17  
18  
19  
20  
21  
22  
23  
24  
25  
26  
27  
28  
29  
30  
31  
32



1 **Table 1.** Models used in this study and their specifications.

Model	Version	Indirect effects included	References
CESM1-CAM5	1.1.2	Sulfate: all indirect effects	Hurrell et al. (2013); Kay et al. (2015)
MIROC-SPRINTARS	5.9.0	Sulfate: all indirect effects	Takemura et al. (2009); Watanabe et al. (2010)
HadGEM3	GA 4.0	Sulfate: all indirect effects	Bellouin et al. (2011); Walters et al. (2014);
NorESM1	NorESM1-M	Sulfate: all indirect effects	Bentsen et al. (2013); Iversen et al. (2013);

2

3

4 **Table 2.** Number of El Niño and La Niña years for each model from coupled baseline and SUL×10Asia

5 simulations in PDRMIP.

Years	CESM1-CAM5 (base)	CESM1-CAM5 (sulx10asia)	MIROC-SPRINTARS (base)	MIROC-SPRINTARS (sulx10asia)	HadGEM3 (base)	HadGEM3 (sulx10asia)	NorESM1 (base)	NorESM1 (sulx10asia)
Niño3.4 > 0.5	16	17	8	15	10	11	12	14
Niño3.4 < -0.5	17	22	6	13	9	9	10	14

6

7

8

9

10

11

12